

Supplementary Information

Structural Bolstering of Metal Sites as Nodes in Metal-Organic Frameworks

Sanjit Das, Daniel E. Johnston, Siddhartha Das*

*Department of Chemistry and Biochemistry, Utah State University
0300 Old Main Hill, Logan, Utah 84322, USA*

* To whom correspondence should be addressed: E-mail: siddhartha.das@usu.edu;
Telephone: 01-435-797-2267; Fax: 01-435-797-3390

1. Materials and methods. Starting materials and solvents were purchased and used without further purification from commercial suppliers (Sigma-Aldrich, Alfa Aesar, VWR, J T Becker). $\text{Co}^{\text{II}}(\text{N-MeIm})_4(\text{NO}_3)_2$ (N-MeIm: N-methyl imidazole), $[(\mu^3\text{-O})\text{Cr}^{\text{III}}_3(\text{CH}_3\text{COO})_6]\text{Cl}$ and $[\text{Ru}_2(\text{CH}_3\text{COO})_4]\text{Cl}$ were synthesized and purified following the literature procedures.¹⁻³ MOFs, viz. HKUST-1,⁴ Ni-MOF-74,⁵ Co-ZIF-9,^{6, 7} Cr-MIL-100⁸ and Ru-BTC-MOF⁹ were synthesized and activated following reported procedures. UV-Vis was recorded with Shimadzu UV-2401 spectrophotometer. ¹H NMR was recorded with a Jeol ECX 300. Powder X-ray diffraction was recorded with Rigaku Miniflex II. Thermal gravimetric analysis was recorded with TA Instruments Q50.

2. General condition for UV-Vis studies with molecular complexes.

2.1 For $\text{Cu}_2(\text{CH}_3\text{COO})_4$, $[\text{Co}(\text{N-MeIm})_4](\text{NO}_3)_2$, $[(\mu^3\text{-O})\text{Cr}_3(\text{CH}_3\text{COO})_6]\text{Cl}$ and $[\text{Ru}_2(\text{CH}_3\text{COO})_4]\text{Cl}$ molecular complexes: A weighed amount of molecular complex was suspended in a water-miscible solvent in which the corresponding complex is insoluble (See Table S1). Then the resulting mixture was stirred for 5 minutes and centrifuged for 30 s to settle down the insoluble residue. After which, the UV-Vis absorbance was recorded from the supernatant solution at characteristic wavelength(s) of the corresponding complex in aqueous solution. Next water was added gradually in μL amounts and after each of the additions the absorbance was recorded following stirring and centrifugation. Following this technique water was added till the absorbance became constant or started decreasing after a maxima was reached.

Table S1: Mass, choice of solvent and characteristic wavelengths that were followed for solvation studies with molecular complexes.

Molecular complex	Weight (mg)	Solvent (volume)	Wavelength(s)
$\text{Cu}_2^{\text{II}}(\text{CH}_3\text{COO})_4$	5.0	Acetone (10 mL)	670 nm
$[\text{Ru}_2^{\text{II,III}}(\text{CH}_3\text{COO})_4]^+$	3.0	Acetone (10 mL)	435 nm
$[\text{Cr}_3^{\text{III}}(\mu^3\text{-O})(\text{CH}_3\text{COO})_6]^+$	5.0	Dioxane (10 mL)	440 nm & 585 nm
[#] $[\text{Co}^{\text{II}}(\text{N-MeIm})_4]^{2+}$	8.5	Dioxane (8 mL)	530 nm & 565 nm

[#] N-MeIm: N-methyl imidazole. ^{*} Co-complex and Cr-complex were sparingly soluble in dioxane.

2.2 For $\text{Ni}^{\text{II}}(\text{CH}_3\text{COO})_2$ molecular complex: As 50 mg $\text{Ni}^{\text{II}}(\text{CH}_3\text{COO})_2$ was dissolved in 8 mL water and then the above mentioned procedure was followed; 14% aqueous ammonia was added instead of water and absorbance was recorded at characteristic wavelength (576 nm) of $\text{Ni}^{\text{II}}(\text{CH}_3\text{COO})_2$ in aqueous ammonia solution.

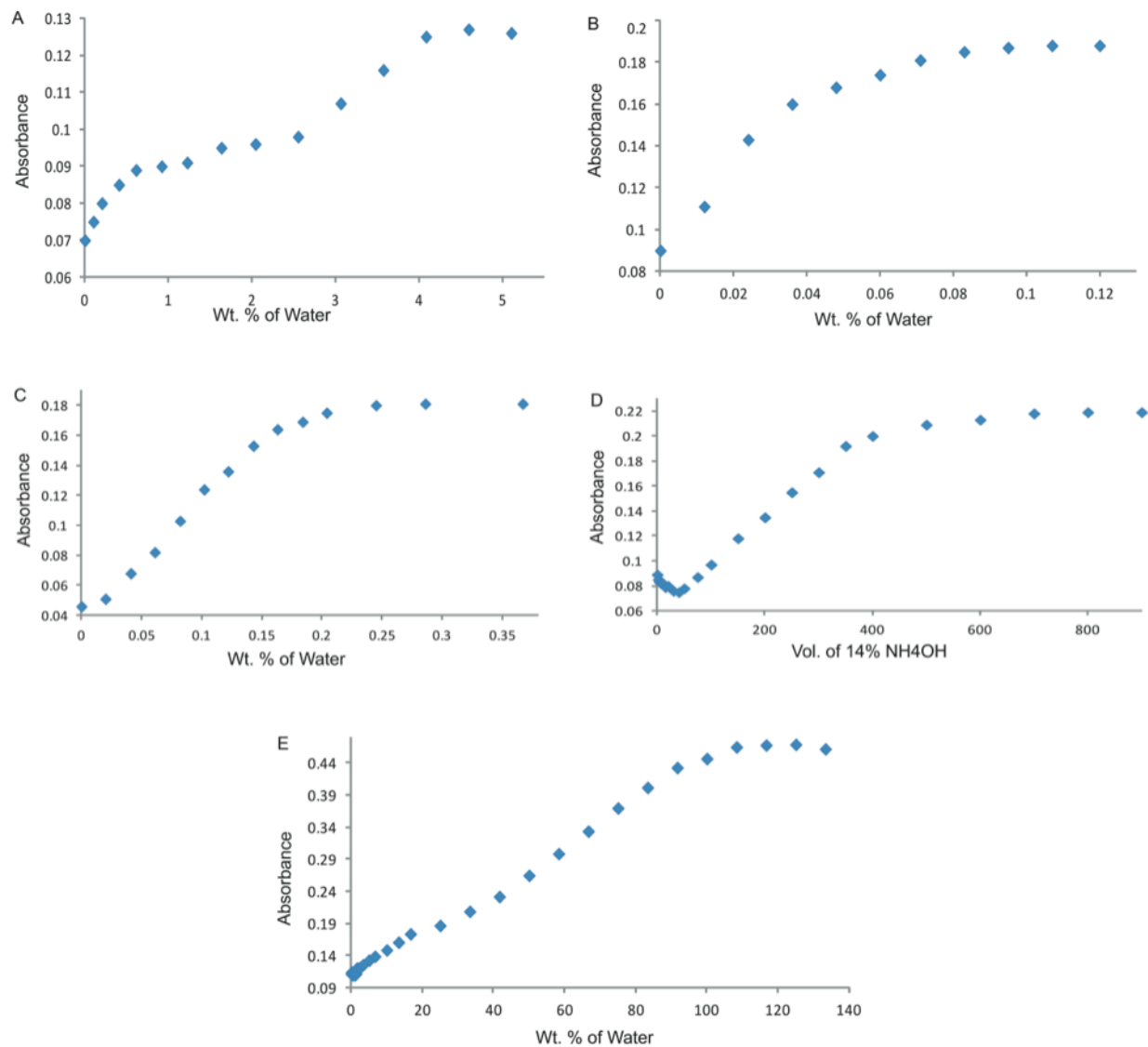


Fig S1. Plots of UV-Vis absorbances resulting from the solvated molecular complexes vs. the wt % of H₂O or volume of NH₄OH added. For molecular complexes: (A) [Cr₃O(CH₃COO)₆]Cl, (B) [Co(*N*-MeIm)₄](NO₃)₂, (C) Cu₂(CH₃COO)₄, (D) Ni(CH₃COO)₂ and (E) [Ru₂(CH₃COO)₄]Cl.

3. General conditions for ^1H NMR studies with molecular complexes. The molecular complexes were taken in $\text{CD}_3\text{C}(\text{O})\text{CD}_3$. Deionized water was added to this suspension. The amount of H_2O used for each molecular complex corresponded to the midpoint of the steep part of the ‘S-curve’ for the respective complex, as derived from their UV-Vis studies (Fig S1). The solution was kept at room temperature for 24 hours and ^1H NMR was recorded (Fig S2).

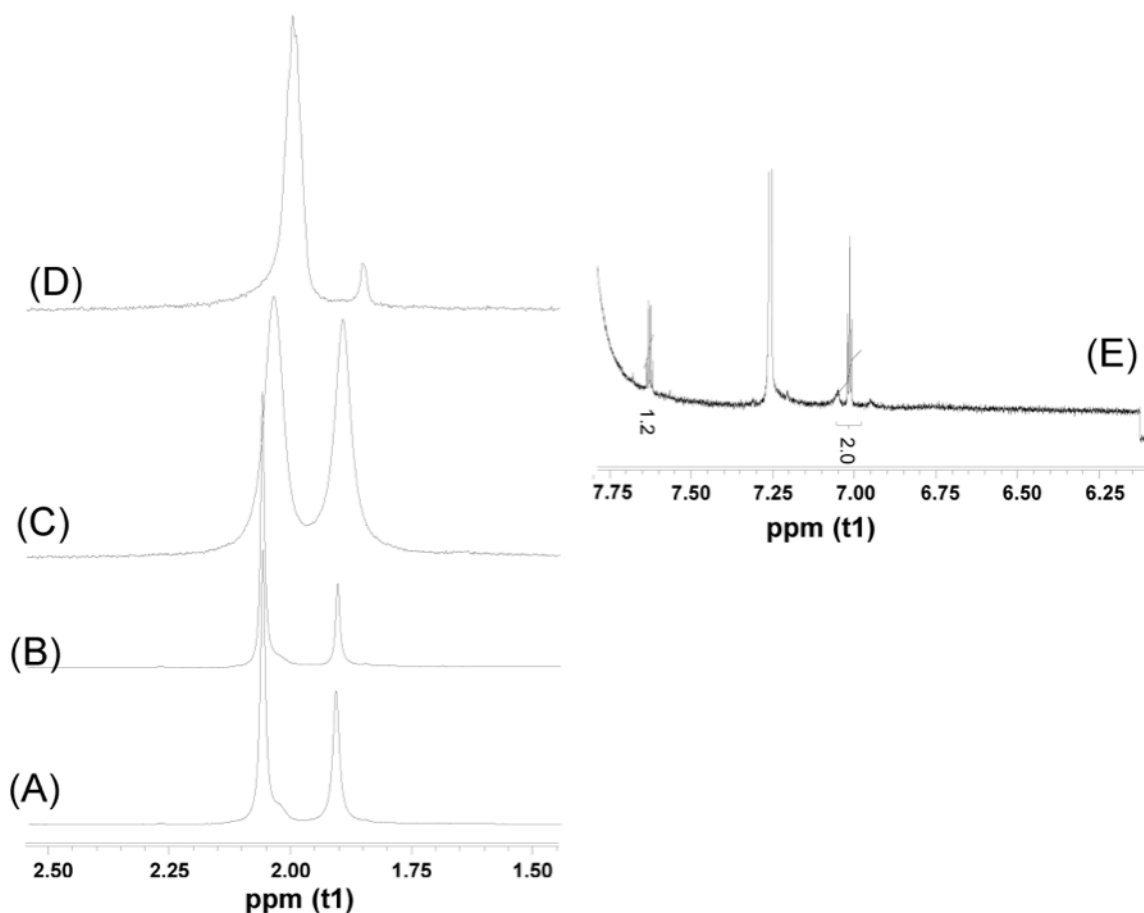


Fig S2. ^1H NMR spectra showing free ligands resulting from the dissociation of metal complexes upon addition of water. The peak at ~ 2.05 ppm corresponds to the residual solvent peak. For, (A) $\text{Cu}_2(\text{CH}_3\text{COO})_4$, (B) $\text{Ni}(\text{CH}_3\text{COO})_2$, (C) $[\text{Cr}_3\text{O}(\text{CH}_3\text{COO})_6]\text{Cl}$ (D) $[\text{Ru}_2(\text{CH}_3\text{COO})_4]\text{Cl}$ and (E) $[\text{Co}(\text{N-MeIm})_4](\text{NO}_3)_2$.

4. General conditions for PXRD studies with MOFs.

4.1 Water stability studies with MOFs: 5 mg of MOF was suspended in the solvent that was used for the corresponding molecular system (Table S1) Water was added gradually in 100 micro L increments; The resulting suspended solution was kept for 15 hours, at room temperature. Then PXRD of remaining residue in the solution was recorded. This was continued till the MOFs start losing characteristic PXRD features. As, other than HKUST-1 none of the tested MOFs lost any crystallinity, even in neat water, we performed the pH variation test as described in section 4.2.

4.2 Resistance to any structural changes at varied pH with Ni-MOF-74, Co-ZIF-9, Cr-MIL-100 and Ru-BTC-MOF: 5 mg MOF was suspended in different pH solutions (pH 3 to pH 10) and kept for 15 hours at room temperature. Then PXRD of the precipitate was recorded.

(The general procedure of the above two studies are depicted in Fig S3)

5. Catalysis with $[\text{Co}(\text{N-MeIm})_4](\text{NO}_3)_2$ and Co-ZIF-9.

The catalytic studies with these were carried out and were followed as described previously.¹⁰

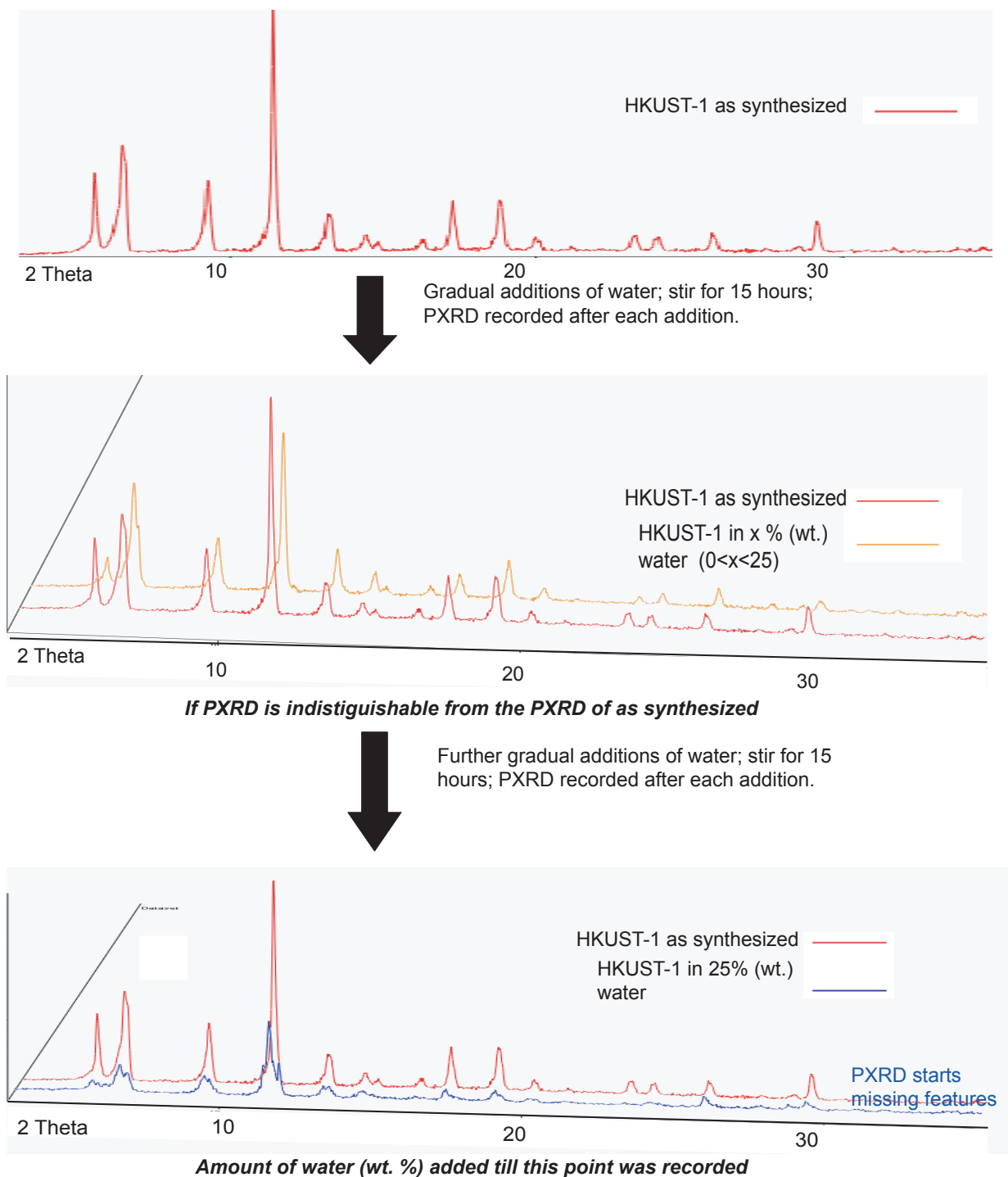


Fig S3. Study of the structural robustness of a metal site in a MOF. PXRD of a sample of MOF was performed upon incremental addition of H₂O or under incremental pH changes. Schematic representation of the study with a representative MOF (HKUST-1) is shown. The same was performed with all other MOFs.

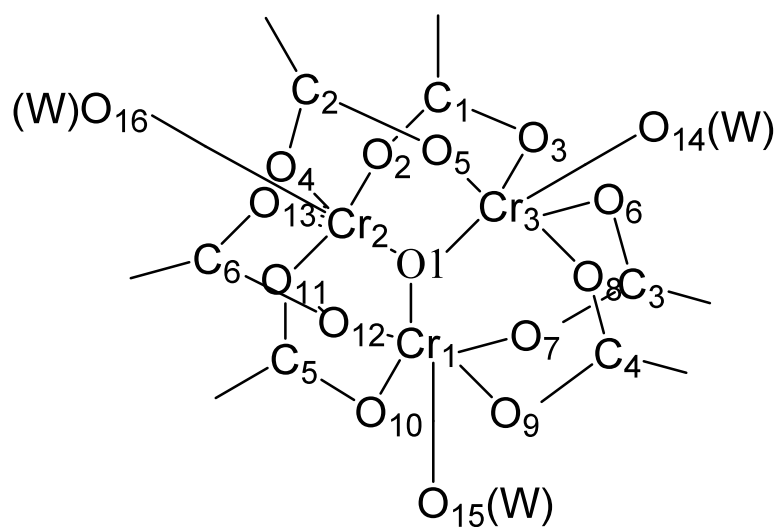
6. Comparison of respective bond lengths and bond angles at the metal sites in molecular complexes vs. MOFs.

Table S2. Copper acetate, Cu-MOP-14 & HKUST-1.^{11,12,4}

	Copper acetate	MOP-14	HKUST-1
<i>Bond lengths</i>			
Cu-Cu	2.6143 Å	2.658 Å	2.628 Å
Cu-O (C) [§]	1.9898 Å	1.972 Å	1.952 Å
Cu-O	2.1613 Å	2.146 Å	2.165 Å
C-O(C) [§]	1.2593 Å	1.257 Å	1.252 Å
<i>Bond angles</i>			
O(C)-Cu-O(C)(trans) [§]	168.9 ⁰	167.5 ⁰	168.2 ⁰
O(C)-Cu-O(C)(cis) [§]	90.60 ⁰	90.9 ⁰	89.40 ⁰
O(C)-Cu-O(C)(cis) [§]	88.30 ⁰	87.7 ⁰	-----
O(C)-Cu-Cu [§]	82.82 ⁰	83.7 ⁰	84.11 ⁰
O(C)-Cu-Cu [§]	86.11 ⁰	83.8 ⁰	-----
C-O(C)-Cu [§]	124.46 ⁰	123.6 ⁰	123.0 ⁰
O(C)-C-C [§]	118.14 ⁰	117.5 ⁰	117.2 ⁰

[§] O(C): carboxylate oxygen atom.

Table S3. Chromium oxy acetate and Cr-MIL-100.^{1,8}



Chromium oxy acetate

Cr-MIL-100

Bond lengths

Cr(1)-O(1)	1.892	1.966
Cr(1)-O(7)	1.959	1.969
Cr(1)-O(12)	1.973	1.967
Cr(1)-O(9)	1.960	1.969
Cr(1)-O(10)	1.983	1.967
Cr(1)-O(15)	2.084	1.953
Cr(2)-O(1)	1.886	1.966
Cr(2)-O(2)	1.995	1.967
Cr(2)-O(11)	1.987	1.969
Cr(2)-O(4)	1.965	1.967
Cr(2)-O(13)	1.963	1.969
Cr(2)-O(16)	2.040	1.953
Cr(3)-O(1)	1.895	1.966
Cr(3)-O(3)	1.964	1.969

Cr(3)-O(6)	1.967	1.967
Cr(3)-O(5)	1.963	1.969
Cr(3)-O(8)	1.972	1.967
Cr(3)-O(14)	2.069	1.953
<i>Bond angles</i>		
O(1)-(Cr1)-O(9)	96.1	92.63
O(1)-(Cr1)-O(10)	94.5	99.86
O(1)-(Cr1)-O(7)	93.1	99.86
O(1)-(Cr1)-O(12)	97.0	92.63
O(1)-(Cr1)-O(15)	177.8	166.36
O(1)-(Cr2)-O(2)	96.2	92.63
O(1)-(Cr2)-O(11)	94.6	99.86
O(1)-(Cr2)-O(4)	95.3	99.86
O(1)-(Cr2)-O(13)	93.8	92.63
O(1)-(Cr2)-O(16)	179.4	166.36
O(1)-(Cr3)-O(3)	94.5	92.63
O(1)-(Cr3)-O(6)	93.1	99.86
O(1)-(Cr3)-O(5)	97.0	99.86
O(1)-(Cr3)-O(8)	96.1	92.63
O(1)-(Cr3)-O(14)	177.8	166.36
Cr(1)-O-Cr(2)	120.3	122.97
Cr(1)-O-Cr(3)	120.2	122.97
Cr(3)-O-Cr(2)	119.5	112.40

Table S4. Ruthenium acetate and Ru-BTC-MOF.^{13,9}

	Ru-acetate	Ru-BTC-MOF
<i>Bond lengths</i>		
Ru-Ru	2.267-2.43	2.599
Ru-O(C) [§]	2.019	1.977
C-O(C) [§]	1.271	1.275
<i>Bond angles</i>		
Ru-Ru-O(C) [§]	89.45	84.93
O(C)-Ru-O(C) [§] (cis)	90	89.44
Ru-O(C)-C [§]	119.4	122.34
O(C)-C-O(C) [§]	122.2	123.8

[§] O(C): carboxylate oxygen atom.

7. Thermal-gravimetric study for molecular complexes.

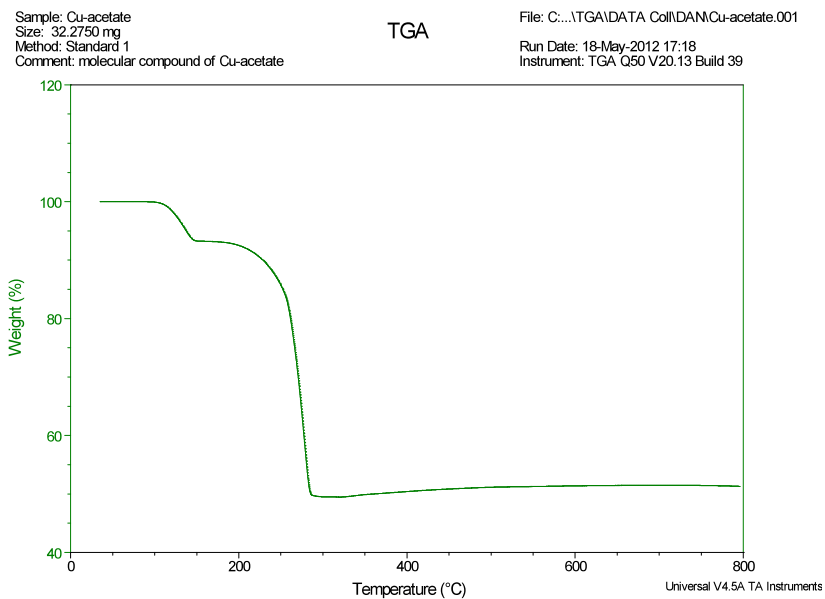


Fig S4. TGA plot for $\text{Cu}_2^{\text{II}}(\text{CH}_3\text{COO})_4$.

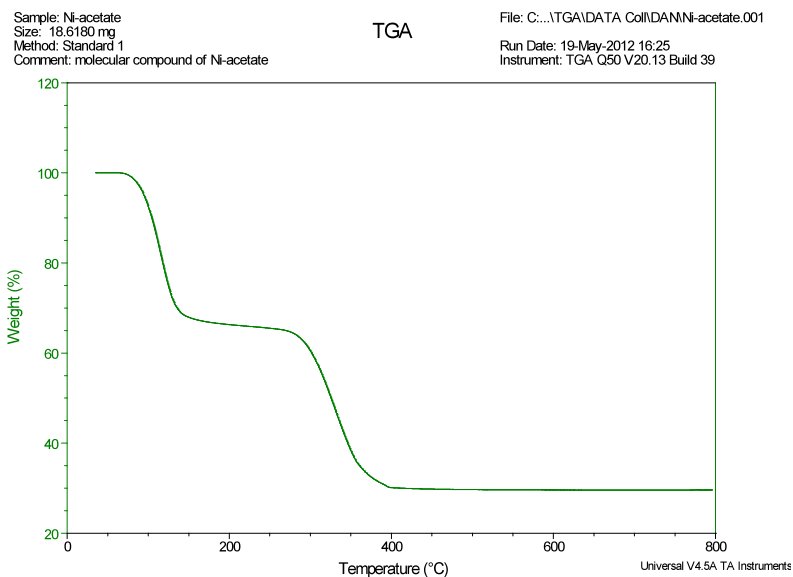


Fig S5. TGA plot for $\text{Ni}_2^{\text{II}}(\text{CH}_3\text{COO})_4$.

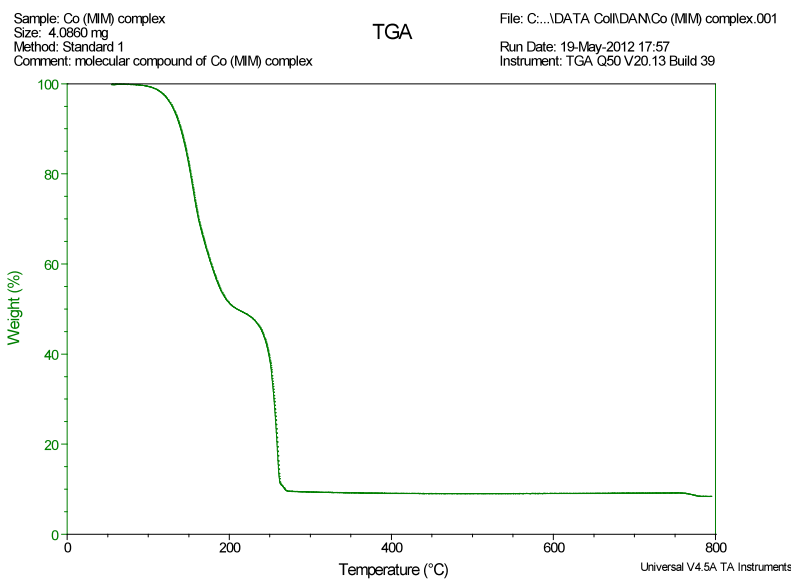


Fig S6. TGA plot for $[\text{Co}(\text{N-MeIm})_4]\text{Cl}_2$.

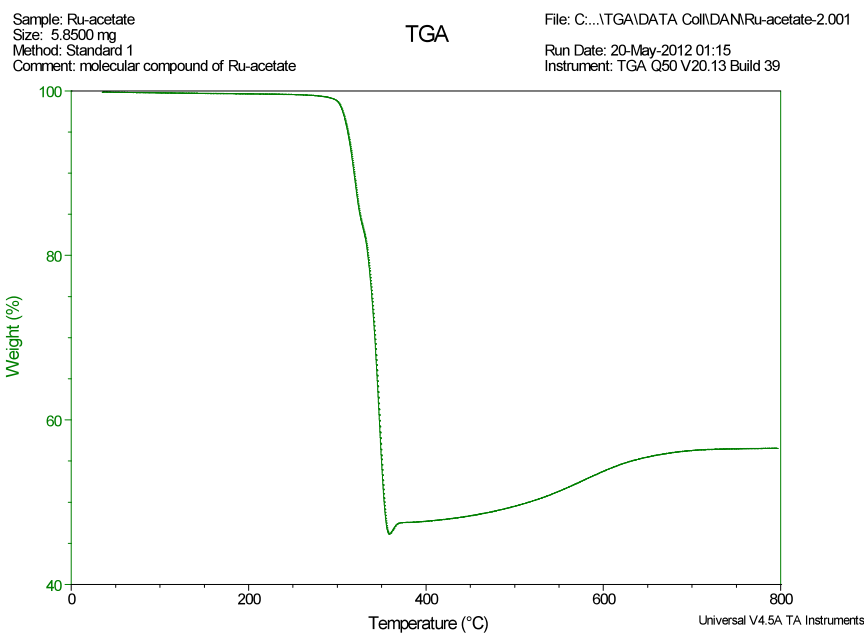


Fig S7. TGA plot for $[\text{Ru}_2(\text{CH}_3\text{COO})_4]\text{Cl}$.

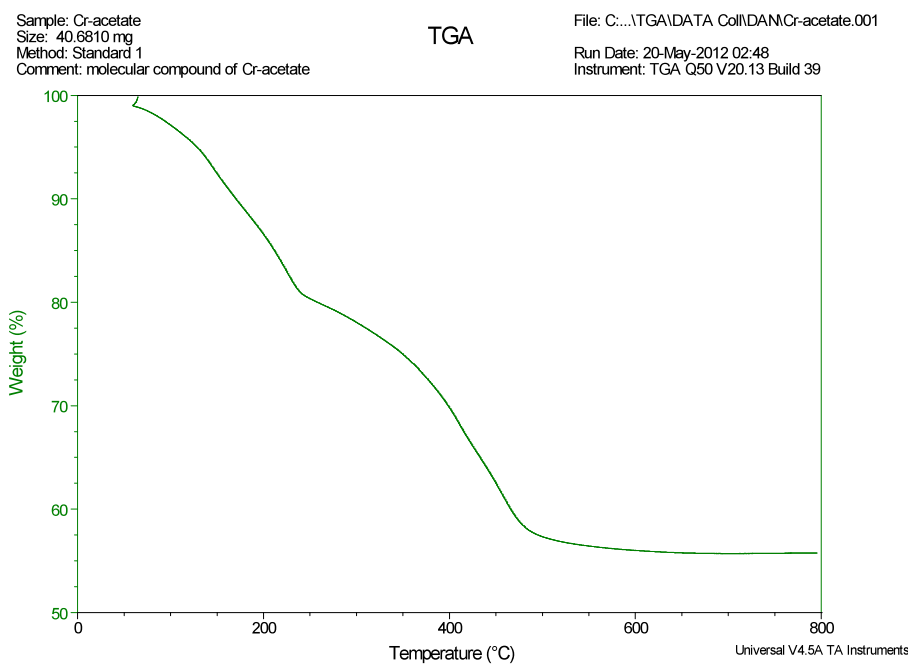


Fig S8. TGA plot for $[\text{Cr}_3(\mu^3\text{-O})(\text{CH}_3\text{COO})_6]\text{Cl}$.

References.

1. T. Fujihara, J. Aonahata, S. Kumakura, A. Nagasawa, K. Murakami and T. Ito, *Inorg. Chem.*, 1998, **37**, 3779-3784.
2. Stephens, T. A. and Wilkinson G., *Journal of Inorganic & Nuclear Chemistry*, 1966, **28**, 2285-&.
3. D. S. Caswell and T. G. Spiro, *J. Am. Chem. Soc.*, 1986, **108**, 6470-6477.
4. S. S.-Y. Chui, S. M.-F. Lo, J. P. H. Charmant, A. G. Orpen and I. D. Williams, *Science*, 1999, **283**, 1148-1150.
5. S. R. Caskey, A. G. Wong-Foy and A. J. Matzger, *J. Am. Chem. Soc.*, 2008, **130**, 10870-10871.
6. K. S. Park, Z. Ni, A. P. Cote, J. Y. Choi, R. D. Huang, F. J. Uribe-Romo, H. K. Chae, M. O'Keeffe and O. M. Yaghi, *Proc. Natl. Acad. Sci. U. S. A.*, 2006, **103**, 10186-10191.
7. J. Zakzeski, A. Debczak, P. C. A. Bruijninx and B. M. Weckhuysen, *Appl. Catal. A-Gen.*, 2011, **394**, 79-85.
8. G. Férey, C. Serre, C. Mellot-Draznieks, F. Millange, S. Surblé, J. Dutour and I. Margiolaki, *Angew. Chem. Int. Edit.*, 2004, **43**, 6296-6301.
9. O. Kozachuk, K. Yusenko, H. Noei, Y. Wang, S. Walleck, T. Glaser and R. A. Fischer, *Chem. Commun.*, 2011, **47**, 8509-8511.
10. L. T. L. Nguyen, K. K. A. Le, H. X. Truong and N. T. S. Phan, *Catal. Sci. Technol.*, 2012, **2**, 521-528.
11. George M. Brown and R. Chidambaram, *Acta Cryst.*, 1973, **B29**, 2393-2403.
12. H. Furukawa, J. Kim, N. W. Ockwig, M. O'Keeffe and O. M. Yaghi, *J. Am. Chem. Soc.*, 2008, **130**, 11650-11661.
13. Avi Bino, F. Albert Cotton and Timothy R. Felthouse, *Inorg. Chem.*, 1979, **18**, 2599-2604.